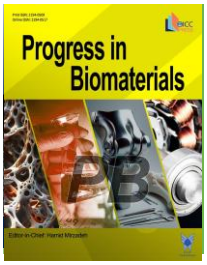

Volume 14, Issue 3, 2025: Article 11

Progress in Biomaterials (PIBM)

https://doi.org/10.57647/pibm-2025-17395

Long-Term in Vivo Response to Biodegradable Anodized Magnesium AZ91 Alloy for Bone Repair

Julieta L. Merlo[1], Sabrina Carrizo[1], Florencia Tano de la Hoz[1], Leandro Salemme Alonso[2], María A. Otaz[3], Josefina Ballarre[1], María R. Katunar[1], Silvia Marcela Ceré[1,*]

[1]*Applied Electrochemistry Area, INTEMA-CONICET, National University of Mar del Plata, Argentina*
[2]*Salemme Implants, Mar del Plata, Buenos Aires, Argentina*
[3]*Private medical Veterinary, CABA, Buenos Aires, Argentina*

***Corresponding author:** jmerlo@mdp.edu.ar

Original Research Article:

Received:
16 May 2025

Accepted:
26 July 2025

Published in issue:
30 September 2025

Abstract

Biodegradable metals, such as magnesium-based alloys, are of great interest for use as intracorporeal implants that disappear once the tissue or function is restored. These materials are even suitable for load-bearing applications, but their degradation rate still needs to be reduced and controlled to avoid hydrogen gas liberation. A surface treatment of anodization has already been described for the magnesium AZ91 alloy, which acts as a barrier to prevent degradation and reduce hydrogen release, showing good *in vivo* results after 30 days of implantation in a murine model. In this study, the performance of anodized AZ91 alloy was evaluated over a long-term period of 6 months in the same animal model. The new bone in contact with the implants exhibited a continuous interface, without gas pockets or fibrous tissue. Bone-to-implant contact was better than that of a polymeric implant (control), and the new bone showed favorable results in terms of volume, trabecular thickness, mineral apposition rate, maturity, and crystallinity. All this evidence supports the potential of anodized AZ91 as a candidate for biodegradable bone fixation devices.

Keyword: AZ91, Biomaterials, Rat model, Surface treatment

Cite this article: Merlo, J. L., Carrizo, S., Tano de la Hoz, F., Salemme Alonso, L., Otaz, M. A., Ballarre, J., Katunar, M. R. & Cere, S. M., Long-Term in Vivo Response to Biodegradable Anodized Magnesium AZ91 Alloy for Bone Repair. Progress in Biomaterials 14(3), Article 11 (2025). https://doi.org/10.57647/pibm-2025-17395

Graphical abstract

1. Introduction

Biodegradable metals are challenging the existing paradigm in biomaterial science by aiming to develop metallic implants that have the adequate degradation and mechanical resistance but only in a limited period of time, and then uniformly corrode in the body environment [1]. The purpose of biodegradable implants is to support tissue regeneration and healing but then completely degrade once the affected tissue is restored. The interest in using biodegradable metals for intracorporeal implants relies on reducing invasiveness and treatment costs. This is particularly important considering the increasing life expectancy of patients, which is associated with a growing demand of implants [2]. In the case of bone repair, magnesium (Mg)-based alloys are outstanding candidates for replacing the use of permanent materials such as titanium alloys or stainless steel [3]. Mg-based alloys exhibit low density and similar-to-compact bone mechanical properties (ductility and elastic modulus), which would prevent *stress shielding* problems [4]. Moreover, its corrosion in aqueous solutions generate non-toxic products for the organism since Mg is an essential element for metabolism and osseous tissue function [5]. This makes them better candidates for bone fixation devices, such us pins and screws, than biodegradable polymeric materials (e.g. polylactic acid, PLA, and polyglycolic acid, PGA), which are unsuitable for load-bearing implants [6]. However, Mg corrosion reaction produces hydrogen gas liberation and local alkalization [7]. If the rate of Mg degradation is excessively rapid or uncontrolled, hydrogen can form gas pockets that then would separate tissues or the implant surface from tissues, both causing pain and local swelling. Local alkalization, in the other hand, is detrimental for pH dependent physiological reactions [8]. To overcome this issue, surface treatments are being studied to generate a barrier between the Mg-substrate and the aggressive environment that allows an optimal rate of corrosion [9] specially at early stages of implantation, avoiding any potential damage to the body. Surface coatings, including inorganic, polymer, and composite coatings have been applied with promising outcomes [10], as well as surface modification techniques such as ion implantation [11] or ultrasonic shot peening [12]. While significant progress has been made, further comprehensive research is required before these systems can be translated into clinical applications. Anodization is one of the widely used strategies to modify metallic surfaces [13]. It consists in an electrochemical process that generates an oxide film on the metal surface, with the aim of retarding the initial burst of corrosion [14]. In a previous study on AZ91 Mg alloy, we demonstrated that low-voltage electrochemical anodizing treatment in 5 mol/L KOH solution generates magnesium oxide/hydroxide on the alloy surface, which acts as a barrier to prevent fast degradation at early immersion or implantation times, reducing the hydrogen release [15]. This treatment improved the *in vitro* biocompatibility of the alloy and induced an adequate short-term *in vivo* response in a murine model [15], [16]. Specifically, new bone formed around anodized AZ91 presented, up to 30 days-post implantation, good characteristics in terms of volume, mineralization and maturity, while gas pockets were not detected [16]. These findings support the anodic oxide film as a promising innovation to overcome the limitations of Mg-based implants, providing a simple, cost-effective, and scalable surface modification capable of reducing early degradation. However, understanding its long-term effectiveness and biological response remains necessary to confirm its suitability for clinical translation. The aim of this study is to describe the performance of the anodized AZ91 Mg alloy after 6 months of implantation in adult rat femur, as a potential biomaterial for bone

10.57647/pibm.2025.17395

fixation devices. Thus, the characteristics of the new bone around implants in terms of mineralization, maturity, morphology, presence of hydrogen gas pockets, and their systemic effects, are described in a rat transcortical model.

2. Materials and methods

2.1. Implant material and anodizing process

Commercial magnesium alloy AZ91D (Al 9.0, Zn 1.0, Fe 0.005, Mn 0.33, Ni 0.002 wt %; MagIC - Magnesium Innovations Center, Germany) extruded sheets of 0.33 cm thickness were cut into pieces of 3.5 to 2.5 × 1 × 1 mm. Pieces were then polished up to 1200 grit with emery paper, rinsed with ethanol, and dried with hot air. Immediately after, anodizing process was performed using a Consort EV231 power source (Belgium), a counter electrode of platinum foil (cathode) and the AZ91D piece as the working electrode (anode), in a potassium hydroxide solution (85%, Biopack, Argentina, 5 mol/L). Anodizing process was performed at low voltage (5 V) for 40 min. Then, the anodized pieces were dried by hot air, and sterilized by dry air (180° C), for 2 h. Anodized pieces ("A-Mg" implants) were stored in sterilized conditions until implantation surgery. Non-anodized AZ91D was excluded as a control material due to ethical considerations, as non-coated Mg or Mg alloys release hydrogen upon implantation, leading to the formation of gas cavities in tissues [17], which can cause pain. Instead, a clinically approved biodegradable material for implantation, PLA, was selected as the control material for the present study. Cylindrical pieces of polylactic acid (PLA; medical grade, donated by INTEMA, Argentina) of 3.5 to 2.5 mm length and 1.5 mm diameter were used as control material ("PLA" implants). Sterilization of these pieces was performed by immersion in 70% ethylic alcohol, for 4 h, immediately prior to implantation.

2.2. Animal model

Male WKAH/Hok rats (n = 10; 263 ± 30 g body weight) were randomly assigned to one of two groups: A-Mg (treatment group) or PLA (control group). Animals were housed in a temperature and humidity controlled room with a 12/12 h light-dark cycle, and feeding *ad libitum*. The distribution of animals in experimental groups, their maintenance, implantation surgery, and euthanasia were carried out in accordance with bioethical protocols, minimizing the number of animals used in accordance with the principle of the 3Rs. All procedures involving animals were approved by the Bioethics Committee of the Natural and Exacts Sciences Faculty of the National University of Mar del Plata (Mar del Plata, June 2017; expedient number 2555-34-17). Rats were anaesthetized with ketamine (Holliday, Argentina; 80 mg/kg of body weight) and xylazine chlorhydrate (Richmond, Argentina; 10 mg/kg of body weight). The surgery region was shaved and cleaned with antiseptic solution. Animals were placed in a supine position and the implantation site was exposed in the middle region of the femur's internal face. A region of around 0.5 cm diameter was carefully scraped and a hole was transversally drilled in the midshaft of the femur using a hand drill at low speed, taking care of not trespassing the drill through the posterior cortical bone. Implant was then placed by press-fit into the hole (Fig. 1). Each rat received two implants (one per femur) of the same material (A-Mg or PLA). The wound was closed with conventional suture. A warm environment was ensured during all surgery and recovery period. Animals received a dose of ketoprofen (Merial, Argentina; 10%, 5 mg/kg of body weight) for pain treatment, monitored until recovery from anesthesia, and then returned to their respective cages. During the following days, animals' social behavior, feeding and hydration were observed on a daily basis, paying special attention to their ability to move their legs.

2.3. Bone labeling with fluorochromes

Pattern and rate of new bone mineralization were assessed through a polychrome sequential fluorescent labeling method. Three and twelve days prior to animal euthanasia, calcein (Sigma-Aldrich, USA; 25 mg/mL; 30 mg/kg of body weight) and alizarin complexone (Sigma-Aldrich, USA; 25 mg/kg; 50 mg/kg of body weight) fluorochromes were intraperitoneally administered to rats. Fluorochromes bind to calcium ions being incorporated at mineralization sites. After animal euthanasia and femurs processing (see below), fluorescent dyes were detected in histological sections with a fluorescence microscope (Nikon Eclipse Ti, Tokyo, Japan) in order to visualize new sites of mineralization and calculate the mineral apposition rate (MAR). The MAR was calculated by measuring interlabel distances in several points on each histological section and then dividing the values by the time interval between administrations of the two fluorescent markers (9 days; [18]). Images were analyzed using FIJI software (opensource: https://fiji.sc/).

2.4. Femurs processing and histological observation

After 6 months of implantation, all rats were deeply anesthetized with Ketamine and Xylazine (80 mg/kg of body weight; 10 mg/kg of body weight, respectively) and euthanized with an intraperitoneal dose of sodic pentobarbital (Brouwer, Argentina; 0.4 g/mL; 90 mg/kg of body weight). Both femurs were retrieved and fixed

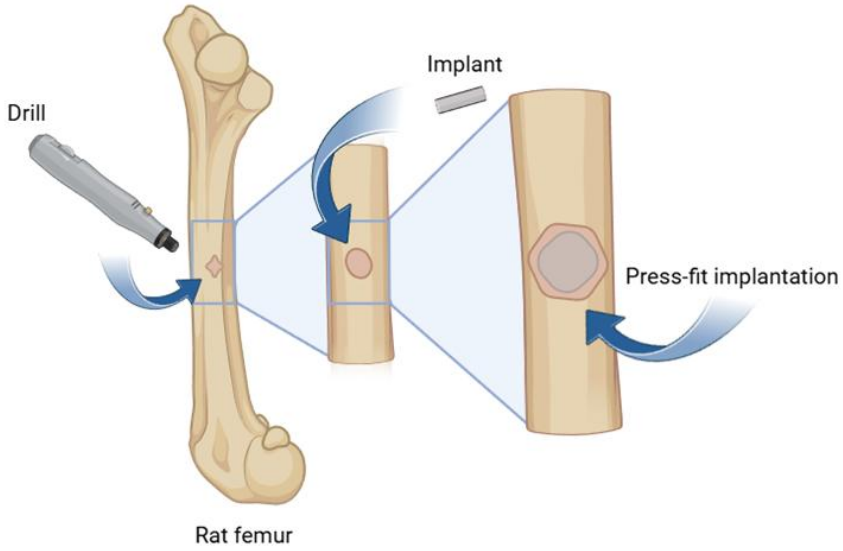

Figure 1. Schematic representation of the surgical procedure done in rat femurs: a transcortical hole was drilled in the midshaft using a low-speed drill, followed by press-fit implantation

in 10% (w/v) neutral formaldehyde buffer for 7 days.Then, femurs were dehydrated in a series of alcohol–water mixtures (70, 85, 96 and 100% vol) followed by immersion in a methacrylated solution, and finally embedded in a polymethyl methacrylate (PMMA; Prothoplast, Subiton Laboratories, Argentina) solution and polymerized. The PMMA blocks were cut with a low-speed diamond blade saw (Buehler GmbH) cooled with vegetal oil, obtaining femur longitudinal cross-sections (transversal to the long axis of the implant) of 100-150 µm thick. Slices where the implant was placed in the medulla were selected for subsequent analyses (3-4 slices per implant), while those where the implant was surrounded by cortical bone were discarded. Selected slices from each femur were first observed using a fluorescence microscope (Nikon Eclipse Ti, Tokyo, Japan) in order to register fluorochromes labeling (see above), using the appropriate filters for each dye. Then, sections were analyzed by Raman spectroscopy (see below). Finally, sections were stained with Toluidine blue, which allows observation and identification of tissues (e.g. bone, bone marrow, fibrous tissue) around the implant, in a light microscope (Nikon Eclipse Ti, Tokyo, Japan). Bone-implant contact (BIC) and histomorphometric analysis of the new bone were performed using FIJI software. For BIC assessment, the length of contact between new bone and the implant surface was registered and expressed as a percentage of the total implant surface length of every histological section. For histomorphometry of the new bone, a region of interest (ROI) was delimited as the 100 µm-thick perimeter area from the implant surface. Total tissue volume (TV), trabecular bone volume (BV) and trabecular bone surface (BS) were registered from each section. With these values, bone volume was calculated as BV/TV (%) = [BV × 100/TV] and trabecular thickness as Tb.Th (µm) = [2/(BS/BV)], following ASBMR standards [19].

2.5. Raman spectroscopic analysis of new bone

The inorganic and organic composition of new bone around implants in non-stained femur sections was characterized by Raman spectroscopy (InVia spectrometer, Renishaw, UK). The spectrometer was equipped with a charge-coupled device (CCD) detector of 1040 x 256 pixels and coupled with a Leica microscope (DM-2500 model; 50x, 0.75 NA) and a computer-controlled x–y–z stage. First, the equipment was calibrated, and a 785 nm diode laser was used as excitation source, in combination with a grating of 1200 grooves/mm. A 50× objective was employed to focus the laser beam onto the sample surface. The laser power was kept at 5% to avoid sample damage, employing one 30-sec acquisition for each data point. The spectra were measured from 300 to 1800 cm^{-1}, with a resolution of 4 cm^{-1}. For each slice, a line scan composed with at least 10 individual spectra was performed, starting from the implant, passing through the newly formed bone and finishing in the bone marrow. The total length of the line scan was variable depending on the thickness of the newly formed bone, and thus spectra points were taken every 1 - 50 µm depending on the sample. A custom developed program was used for spectra analysis [20], [21]. Background fluorescence was first removed by a

modified polynomial fitting algorithm. Then, intensities corresponding to amide I (1643 cm^{-1}), B-type carbonate (1071 cm^{-1}), *v*1 phosphate (960 cm^{-1}), and *v*2 phosphate (430 cm^{-1}) were recorded. With these values, mineral to matrix ratio was calculated as the ratio of the *v*1 phosphate peak to the amide I peak, and carbonate substitution in the lattice structure of the apatite was assessed as the ratio of the B-type carbonate peak to the *v*2 phosphate peak [22]. Finally, mineral crystallinity was determined as the inverse of the width of the *v*1 phosphate (960 cm^{-1}) band at half of the maximum intensity value [23]. The parameters obtained after Raman analysis in the new bone were compared among the implanted materials.

2.6. Mg content in urine

To determine whether A-Mg implant degradation affects animal metabolism due to the systemic release of magnesium ions, urine samples were collected from all rats at 140 days post-implantation. Rat urine collection for qualitative analysis technique was adapted from [24]. This procedure is called the single animal method (SAM) and consists of allowing a single rat to urinate on a plastic wrap placed inside a clean animal cage that was intended to perform this procedure. Once the animal has urinated, it is immediately removed from the cage and the urine is collected with a sterile syringe. The sample is transferred to a micro-centrifuge tube and stored in a freezer for further analysis. A urine volume of 0.5 to 1 mL was obtained from each rat within seconds of their introduction to the cage. The Mg-color kit (Wiener Lab, Argentina) was used for colorimetric detection of magnesium in each sample by duplicate, using a UV spectrophotometer (UV-3600 plus, Shimadzu, Japan), following manufacturer' instructions.

2.7. Leukocyte profile

Relative abundance of each leukocyte type in blood provides information about systemic processes such as stress, allergies, endocrine disorders, chronic infection or inflammation [25]. Blood smears were performed with drops of blood collected from the femoral vein of rats immediately after euthanasia. Smears were fixed with ethyl alcohol, stained with Color Fast Kit (Biopack, Argentina), and then examined under oil immersion at 1000x magnification (Olympus BH-2, Tokyo, Japan). The "wandering technique" [25] was used to record the abundance of each leukocyte type based on their morphology until a total of 200 leukocytes had been examined, and results were expressed as percentage (%). To calculate the total leukocyte abundance, the number of leukocytes encountered in 30 fields in which there was a single layer of erythrocytes was recorded (equivalent to a total of 25,000 erythrocytes; data not shown).

2.8. Statistical analyses

Data is shown in the form of mean value ± S.D. Differences between implant materials and time points studied were assessed by two-ways ANOVAs and Tukey tests. Raman data was analyzed using Mixed Model ANOVA. All tests were performed in STATISTICA 7 software using $p < 0.05$ to reject the null hypothesis.

3. Results

3.1. Clinical observations

Eight animals from a total of ten fully recovered after surgery and were able to walk within a few hours. Throughout the experimental period, no signs of infection or inflammation were observed. The animals exhibited normal behavior and none of them lost body weight during the experimental period. The remaining two animals were not considered for the study since one of them died under anesthesia and the other was euthanized after 3 months post-surgery due to the development of an abdominal tumor (according to a histopathological analysis, data not shown).

3.2. Histological and histomorphometric analysis

Typical images of new bone stained with Toluidine blue around each implant material are shown in Figure 2. From stained sections it was observed that the newly formed bone surrounding both A-Mg and PLA implants was mostly continuous. No fibrous tissue was detected in any histological section, for both materials. There was also no evidence of gas pockets that could potentially result from magnesium degradation (Fig. 2 (A)). BIC measurements revealed that almost all new bone surrounding A-Mg implants was in direct contact with it, while in the case of PLA, BIC was significantly lower (T-test, p = 0.026, Fig. 2 (A, B)). Histomorphometric analyses showed that new bone volume and trabecular thickness formed around A-Mg implants tended to be higher compared with those around PLA (Fig. 2 (C, D), although differences were not statistically significant (p = 0.072, p = 0.13, respectively).

3.3. Fluorochromes labeling

Fluorescent labelling at different time points was used to monitor bone mineralization around implants. Calcein (green fluorescence) and Alizarin complexone (red fluorescence) administered 3 and 12 days before euthanasia respectively, were detected in all animals. Fluorescence was found in segments in outer and inner borders of new bone around implants, in a similar pattern

for both types of materials (Fig. 3 (A). The MAR values obtained did not show statistically significant differences between materials (T-test, p = 0.059, Fig. 3 (B)), although a tendency to a higher MAR was observed in A-Mg compared with PLA.

3.4. Raman spectroscopic analysis of new bone

Ratio of mineral to matrix composition, degree of carbonate substitution in hydroxyapatite lattice, and crystallinity of the hydroxyapatite at the new bone were calculated based on the intensities of phosphate, amides and carbonate peaks from Raman spectra (Fig. 4). These values were extracted from all tissue sections where the peak at 960 cm^{-1} (ν1 phosphate) was detected, to ensure that spectra corresponded to a bone area, and 3-8 spectra per tissue section were included in the analysis. The three parameters studied -mineral to matrix composition, carbonate substitution and crystallinity- did not differ between bone around A-Mg in comparison with PLA (mixed model ANOVAs, p = 0.85, p = 0.67, p = 0.45, respectively). Table 1 shows mean values obtained for these parameters. A detailed summary of the numerical data obtained from histological sections is provided in Supplementary Table 1.

3.5. Mg content in urine

Mg concentration in urine of rats implanted with A-Mg was 24.1 ± 1.2 mg/dL, while the value for rats implanted with PLA was 21,8 ± 4,1 mg/dL. Statistically significant differences were not detected (T-test, p = 0.4).

3.6. Leukocyte count

Leukocyte formula, indicative of inflammatory and infectious processes, did not differ between groups of rats (T-tests, all p > 0.05; Fig. 5).

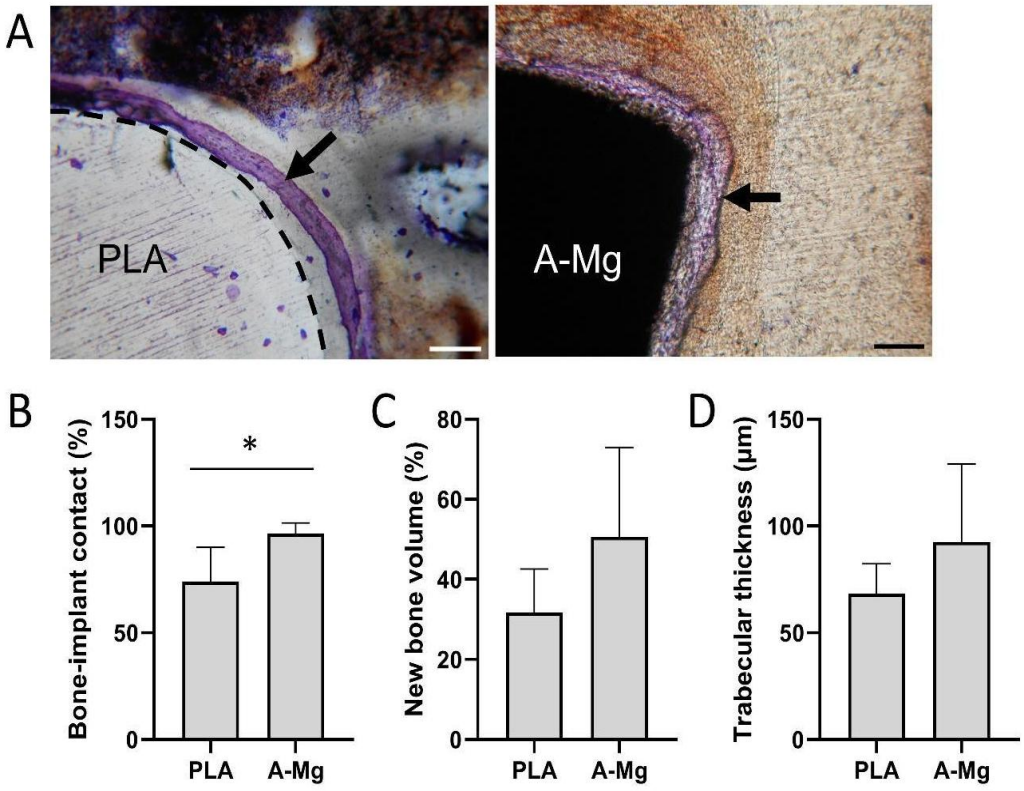

Figure 2. (A) Light micrographs of bone (arrow)-implant (PLA or A-Mg) interface in rat femur cross-sections after 6 months of implantation, stained with Toluidine blue. Dashed line highlights the limits of PLA implant. Scale bar = 200 µm. (B) Bone-to-implant contact, (C) volume of new bone and (D) trabecular thickness parameters obtained by histomorphometric analyses of light micrographs. Asterisk denotes significant differences among groups

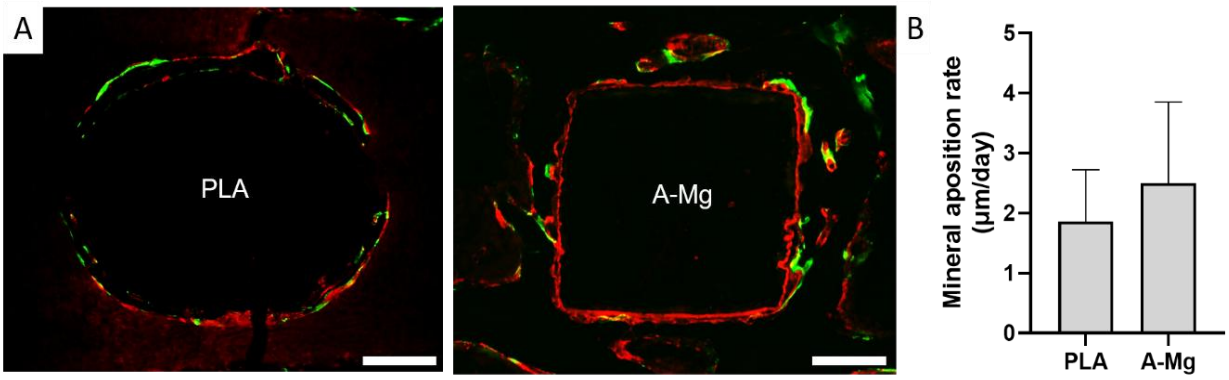

Figure 3. (A) Fluorescence microscopic images of rat femurs cross sections implanted with control PLA or anodized AZ91 for 6 months. Green (calcein) and red (alizarin complexone) labels denoted the sites of mineralization in the new bone. Scale bar = 500 µm. (B) MAR calculated based on calcein and alizarin complexone labels

Table 1. Values of mineral to matrix ratio, carbonate substitution and crystallinity of new bone around control (PLA) or anodized AZ91 (A-Mg) implants

	Mineral to matrix ratio (ν_2 PO_4^{3-}/amide III)	Carbonate substitution (CO_3^{2-} / ν_2 PO_4^{3-})	Cristallinity (based on ν_1 PO_4^{3-})
PLA	1.11 ± 0.63	0.51 ± 0.29	$7.17 \pm 2.39 \times 10^{-4}$
-Mg	1.21 ± 0.39	1.13 ± 0.86	$9.41 \pm 3.48 \times 10^{-4}$

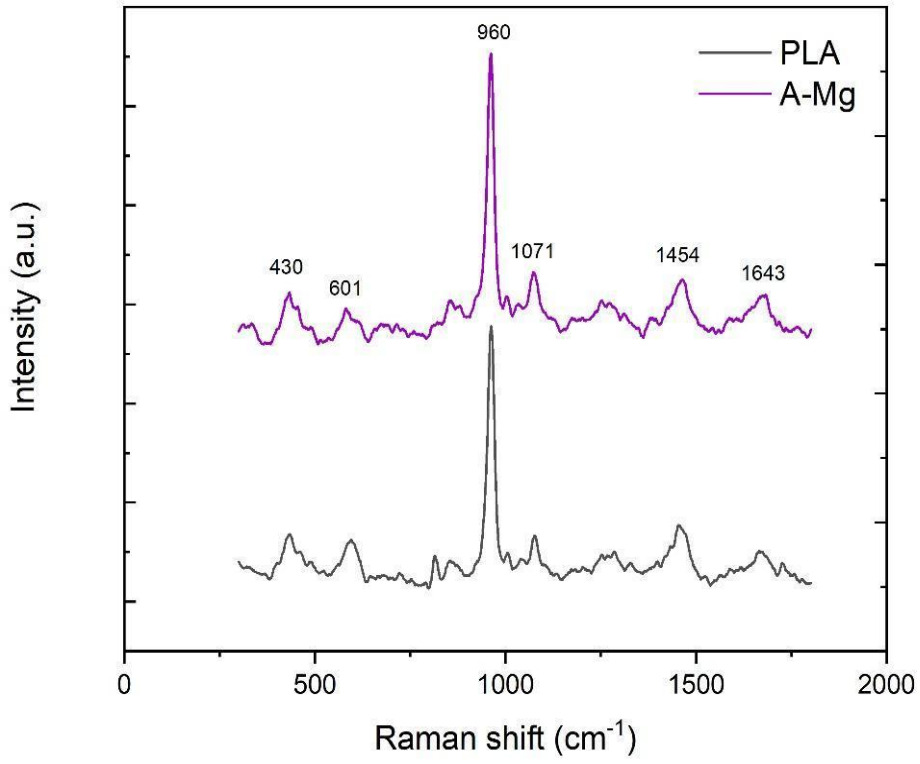

Figure 4. Raman spectra of new bone in PLA and A-Mg implanted zones

10.57647/pibm.2025.17395

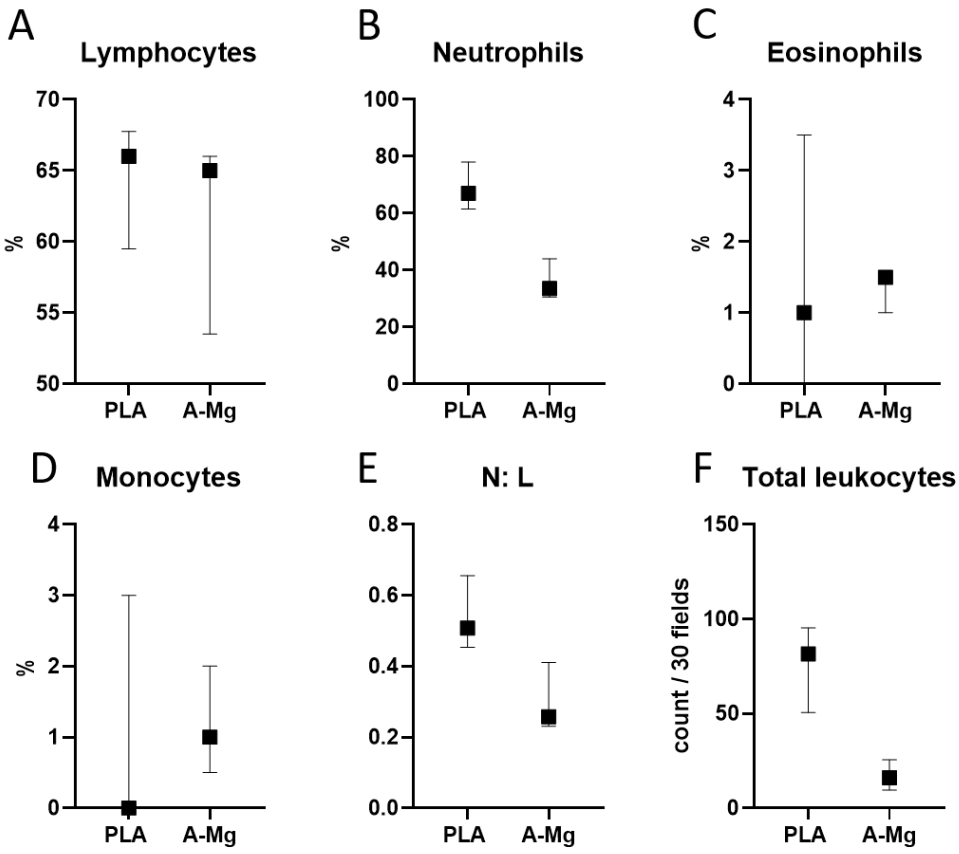

Figure 5. Leukocyte formula (A-D), neutrophil to lymphocytes ratio (E) and total leukocytes count (F) in blood of rats implanted with PLA or anodized AZ91 (A-Mg), at 6 months post-implantation

4. Discussion

One of the core innovations explored in this study is the use of a low-voltage anodic oxide film on AZ91 alloy to modulate early degradation kinetics. This study aimed to explore the long-term behavior of an anodized AZ91 alloy *in vivo*, motivated by the fact that *in vitro* studies, although they provide important information on various aspects of biomaterial corrosion and degradation, still do not represent the complexity of the *in vivo* environment [26]. From a short-term study in rats, we collected valuable insights into the post-implantation period of the anodized AZ91. It promotes the initial formation of woven bone that progresses towards lamellar bone over time, with no detectable tissue rejection responses [16]. However, given that Mg-based temporary implants are expected to reside in the human body for several months to years [27], longer study periods are essential to guarantee safety and identify relevant tissue responses. While this study sheds light specifically on the anodized AZ91, it contributes significantly to the broader understanding of Mg-based biomaterial behavior *in vivo*, particularly after several months' post-implantation. It is worth to point out that an anodically treated Mg-based alloy is presented instead of a biodegradable polymeric material since the bone fixation application requires the mechanical resistance of a material exposed not only to corrosion but to complex load-bearing environments [28]. Through Toluidine blue staining, it was determined that, in general terms, the bone developing around the anodized AZ91 implant is mature, lamellar bone, that covers the implant surface in a continuous manner. Interruptions in bone tissue due to gas pockets that could be generated by the release of hydrogen gas were not detected. In addition, fibrous tissue was not detected in any sample at 60 days post-implantation, in contrast with day 7 when it was found in contact with the anodized surface of AZ91 implant [16]. The presence of this kind of tissue encapsulating a biomaterial result in improper fixation and can lead to implant failure. Combining the findings of this study and previous research [16], it is inferred that fibrous tissue formation may occur during the initial healing phase after anodized AZ91 implantation, characterized by the development of woven bone—a specialized connective tissue abundant in collagen, crucial for stabilizing the injured area—around the implant. Subsequent resorption of this initial woven bone leads to remodeling into lamellar bone [29]. At day 15 and 6 months post-implantation, only lamellar bone is observed around A-Mg implants (and controls), without fibrous tissue, which would indicate a low risk

of implant encapsulation and rejection [30]. One important aspect for a bone –fixation device is its direct bone-to-implant contact, crucial for the success of the implant therapy [31]. Primary stability is associated with the implant design and its mechanical engagement that ensures the absence of micromotion. But a second level of stability has to be provided by the interaction with the tissues, where bone regeneration and remodeling occurs in an equilibrium surrounding the implant [31]. The BIC measurement in this study showed that this contact is higher in A-Mg implants compared with PLA (96% vs. 74%, respectively). The almost complete BIC seen in the bone around anodized AZ91 can be attributed in part to its roughness, since there is evidence that increasing the implant surface roughness improves the mechanical attachment of the implant to the surrounding bone [32]. In the case of the anodized AZ91, it has been previously proven that oxides formed through the superficial treatment of anodization increases the roughness of the AZ91 alloy (Ra_{AZ91} = 0.14 µm vs. $Ra_{A\text{-}AZ91}$ = 2.2 µm, Rz_{AZ91} = 1 µm vs. $Rz_{A\text{-}AZ91}$ = 13 µm), and that cell attachment and viability also increases in comparison with the sandblasted alloy [15]. At this respect, there is a general consensus in that rough surfaces are better for inducing osteoblast adhesion, proliferation and matrix synthesis [33]. The chemical composition of the surface is another factor influencing the interaction with cells and tissues, through its capacity to bind water molecules and proteins. In this respect, anodization produces hydrophilic surfaces that would favor protein adsorption [33], which, in turn, promotes subsequent cellular adhesion. This initial synergistic influence of surface chemistry and topography favoring the interaction with cells and tissues might be responsible for the consequent almost complete bone-to-implant contact detected at 6 months after implantation in A-Mg cases. It should be noted that the mechanical strength and stiffness of PLA are significantly lower than those of magnesium alloys such as AZ91. This discrepancy may influence the local mechanical environment, which is known to modulate bone regeneration processes [34]. PLA, being a relatively soft and non-load-bearing polymer, might lead to a different load transfer in the surrounding bone compared to the metallic implant. As a result, the higher BIC observed for anodized AZ91 may not only reflect its superior surface characteristics, but also a favorable mechanical stimulus for osteointegration.

Histomorphometric analysis of the implanted zones provided quantitative information about the induction of new bone formation. Although it was not statistically significant, a tendency to higher bone volume was observed for anodized AZ91 (A-Mg) in comparison to PLA samples. Histological slices presented variation in bone volume parameter among experimental animals, but, in general, new bone volume around anodized AZ91 was approximately 50% of the total tissue volume, while approximately 32% was detected around PLA implants. These values represent, for both groups, an increase in time in comparison with the percentages obtained from rats implanted for 30 days, where 17.4% and 13.5% of new bone was registered for anodized AZ91 and PLA implants, respectively (Merlo et al. 2021). This means that anodized AZ91 would outperform PLA at long times of implantation, which may be associated with multiple factors inherent to the material. One factor could be the surface roughness achieved through anodization, which enhances osteoblast adhesion and promotes matrix production, as previously discussed. Additionally, the gradual release of magnesium ions from the AZ91 alloy may exert an osteogenic effect. Several studies have reported that Mg^{2+} ions can stimulate the proliferation and differentiation of osteoblasts, as well as promote angiogenesis, all of which are key elements in bone regeneration [35], [36]. The synergy between these physical and chemical cues may underlie the observed differences in bone volume, even though further studies would be required to identify each factor contribution. Other authors also compared the *in vivo* performance of Mg alloys versus PLA. Witte et al. described that implantation of four different Mg alloys resulted in higher mineralized bone than PLA in guinea pigs, after 4.5 months of implantation [37]. However, Kawamua et al. found no differences in bone volume around AZ31 Mg alloy in comparison with PLA in rats, after 3 months [38]. In comparison with titanium, Castellani et al. found similar results regarding a Mg–Y–Nd–HRE alloy and PLA implanted in rats for 6 months [39], and Kawamua et al. described no differences with the bone volume around AZ31 Mg alloy in rats implanted for 3 months [38]. All of these findings suggest that Mg-based materials, such as anodized AZ91, stimulate bone formation to a similar or even superior extent as titanium and PLA, particularly over longer implantation periods. Titanium and PLA are two materials frequently used in medical devices but fail to possess appropriate characteristics for biodegradable bone fixation devices, such as non-degradability and insufficient strength and toughness, respectively. In this sense, these results are promising and future research regarding Mg-based alloys degradation are required to confirm its suitability as biodegradable devices. Although a tendency towards higher MAR could be observed in anodized AZ91 implanted animals, values were not statistically different to PLA-implanted ones. Mean values of ~2 and ~2.5 µm/day were registered for anodized AZ91 and PLA implanted animals, respectively. It is interesting to note that, in our previous study at 7, 15, and 30 days post-implantation, the MAR

could not be quantified as the fluorochromes were overlapping in several areas [16]. Thus, the current study at 6 months post-implantation reveals that the bone tissue around anodized AZ91 and PLA implants increases its mineralization rate over time, at least up to the point studied here. The MAR values detected in the present study are consistent with the magnitudes found in previous research on other biomaterials for bone repair [40], [41]. Raman spectra permitted to determine bone quality regarding the ratio of mineral to matrix composition, the degree of carbonate substitution and crystallinity [42], [20]. The results from the new bone area around either PLA or anodized AZ91 showed similar band intensities. Tissue sections selected for analysis showed a peak at 960 cm^{-1}, associated with the inorganic components of bone, phosphates in apatite. Other binding vibration of phosphates was detected at 430 cm^{-1}, but in lower intensities, as expected based on the literature [20]. B-type carbonate substituted apatite, a component indicative of maturity of bone (Kazanci et al. 2006), was detected in all sections with the distinctive peak for carbonates at 1071 cm^{-1}. Similarly, the C = O vibration associated with amide I, present in the collagen matrix of new bone [43], was observed at 1643 cm^{-1}, generally as a wide band of low intensity. Bands that correspond with the embedding solution, PMMA, were also registered at 601 and 1454 cm^{-1}. Values registered for phosphate, amides and carbonate peaks were used to calculate the ratio of mineral to matrix composition, the degree of carbonate substitution and crystallinity of the new bone around implants. Ratio of mineral (phosphate) to matrix (amide) composition allows for the estimation of the level of mineralization of bone, a complex process that involves the deposition of calcium and phosphates in the bone matrix, forming hydroxyapatite crystals [44]. Carbonate ions can substitute phosphates in the crystals, which could lead to an improvement on the mechanical properties of bone [45]. The value of crystallinity, on the other hand, indicates the degree of maturity and elongation of the apatite crystals, which also affects bone mechanics [23]. All these parameters were statistically similar between PLA and anodized AZ91, and thus both materials would induce a similar level of bone maturity at 6 months post-implantation. As the purpose of biodegradable implants is to completely degrade once the affected function or tissue is restored, it is also important to evaluate the potential systemic effects of the metabolism of degradation products. In this study, Mg content in urine and leukocyte formula were used as indicatives of the systemic state of animals, in addition to the daily observation of their behavior and general aspect. Magnesium content in urine of rats implanted with anodized Mg was similar to those implanted with PLA, indicating that Mg ions metabolism is too low to be detected in urine. Similarly, other authors found unaltered levels of Mg in serum of rabbits implanted with ZEK100 Mg alloy, during a period of up to 12 months [46]. The leukocyte formula of rats implanted with anodized Mg and PLA was also similar in the present study, indicating no inflammatory or allergic reactions to the materials. Other studies also reported no effects on blood cells count of Mg alloys in rats, after 6 months of implantation (Mg-Zn-Mn alloy, [47]; Mg–Y–Nd–HRE, [39]). Overall, systemic effects of Mg-based alloys are null or minimal at long times post-implantation, an important aspect for biodegradable implants. However, as could be seen in histological sections, anodized AZ91 pins were still present after the experimental period of 6 months, and thus longer times of study are required to ensure that the complete degradation process is analyzed. This is consistent with previous reports indicating that Mg-based implants, particularly those treated to reduce corrosion, may require periods longer than 6–12 months to fully degrade *in vivo* [48], [49]. The anodic oxide layer, while effectively reducing early-stage degradation and hydrogen release, may prolong the resorption time of the material. Future studies with extended implantation periods and quantification of implant material loss are needed to accurately determine the total degradation time of anodized AZ91 and to better understand the degradation kinetics in relation with the observed biological responses.

5. Conclusions

The present study evaluated the *in vivo*-long term performance of the AZ91 alloy with an anodizing surface treatment, aimed to reduce initial corrosion and hence decrease hydrogen gas evolution and local alkalization. Through a transcortical implantation of anodized AZ91 and PLA as control in adult Wistar rats, new bone formation and systemic effects were studied after 6 months of implantation. The new bone exhibited a continuous interface in direct contact with the anodized AZ91 pin, without gas pockets or fibrous tissue. Importantly, the bone-to-implant contact was almost complete (96%) for anodized AZ91, and higher than the case of PLA. This improvement in BIC would represent a higher expectation of recovery in patients, as the risk of implant micromotion, which can lead to its failure, is lower. Other characteristics of the newly formed bone around A-Mg implants such as volume andtrabecular thickness, MAR, maturity and crystallinity, were similar to those found for PLA –a material widely used in biodegradable medical applications that do not involve load-bearing support-. Moreover, no detrimental

systemic effects were observed based on the analysis of Mg content in urine and blood cell counts. In conclusion, based on the BIC, the capacity of bone formation, and absence of systemic effects, anodized AZ91 is a promissory candidate for degradable bone fixation devices. This study highlights the potential of anodic oxide films as a strategic surface modification for biodegradable metallic implants, providing a simple and scalable means to tune the early host response.

Acknowledgments

Thanks to A. Cisilino for his help with the customized program for Raman analysis. Funding was provided by the Argentinean Council for Scientific and Technical Research (CONICET; PIP 572, PUE073), and the National University of Mar del Plata (Project 15/G331ING337/12).

Competing interests

The authors have no relevant financial or non-financial interests to disclose.

Authors contributions
All authors contributed equally to the conception, design, execution, and writing of this work. All authors read and approved the final manuscript.

Availability of data and materials
The datasets generated during and/or analyzed during the current study are available from the corresponding author on reasonable request.

Conflict of interests
The authors declare that they have no known competing financial interests or personal relationships that could have appeared to influence the work reported in this paper.

References

[1] Ravoor, J., Thangavel, M., & Renold Elsen, S. (2021). Comprehensive review on design and manufacturing of bio-scaffolds for bone reconstruction. *ACS Appl Bio Mater*, 4:8129–8158.

[2] Pandey, A., Awasthi, A., & Saxena, K.K. (2020). Metallic implants with properties and latest production techniques: a review. *Adv Mater Process Technol*, 6:405–440.

[3] Nasr Azadani, M., Zahedi, A., Bowoto O.K., & Oladapo B.I. (2022). A review of current challenges and prospects of magnesium and its alloy for bone implant applications. *Prog Biomater*, 11:1–26.

[4] Esmaily, M., Svensson, J.E., Fajardo, S., et al. (2017). Fundamentals and advances in magnesium alloy corrosion. *Prog Mater, Sci* 89:92–193.

[5] Saris, N-EL., Mervaala, E., Karppanen, H., et al. (2000). Magnesium: an update on physiological, clinical and analytical aspects. *Clin Chim Acta*, 294:1–26.

[6] Huang, B., Yang, M., Kou, Y., & Jiang, B. (2024). Absorbable implants in sport medicine and arthroscopic surgery: A narrative review of recent development. *Bioact Mater*, 31:272–283.

[7] Song, G. (2005). Recent progress in corrosion and protection of magnesium alloys. *Adv Eng Mater*, 7:563–586.

[8] Song, G. (2007). Control of biodegradation of biocompatable magnesium alloys. *Corros Sci*, 49:1696–1701.

[9] Chen, H., Wang, Y., He, L., et al. (2025). Surface engineering of biodegradable magnesium alloys as orthopedic implant materials: Recent developments and future prospects. *Coatings*, 15:191.

[10] Wang, X., Guo, L., Liu, X., et al. (2024). Enhanced corrosion resistance and cell activity of magnesium alloy by DCPD/MgHPO4·3H2O coating via one-step chemical conversion. *Surf Coatings Technol*, 476:130228.

[11] He, T., Liu, X.H., Xiao, Z.J., et al. (2025). The mechanisms of varying doses of metal ion implantation (Ag, Ti and Zr) on microstructure and properties of pure magnesium. *Rare Met*, 1–18.

[12] Han, M., Du, J., Chen, Y., et al. (2024). Influence of ultrasonic shot peening on the microstructure and corrosion behavior of AZ80M magnesium alloy. *J Alloys Compd*, 980:173633.

[13] Tano de la Hoz, M.F., Katunar, M.R., González, A., et al. (2019). Effect of anodized zirconium implants on early osseointegration process in adult rats: a histological and histomorphometric study. *Prog Biomater*, 8:249–260.

[14] Gray, J.E., & Luan, B. (2002). Protective coatings on magnesium and its alloys - A critical review. *J Alloys Compd*, 336:88–113.

[15] Moreno, J., Merlo, J.L., Renno, A.C., et al. (2023). In vitro characterization of anodized magnesium alloy as a potential biodegradable material for biomedical applications. *Electrochim Acta*, 437.

[16] Merlo, J.L., Katunar, M.R., Tano de la Hoz, F., et al. (2021). Short-term in vivo response to anodized magnesium alloy as a biodegradable material for bone fracture fixation devices. *ACS Appl Bio Mater*, 4:7123–7133.

[17] Witte, F., Fischer, J., Nellesen, J., et al. (2010). In vivo corrosion and corrosion protection of magnesium alloy LAE442. *Acta Biomater*, 6:1792–1799.

[18] Schilling, T., Mueller, M., Minne, H.W., & Ziegler, R. (1992). Mineral apposition rate in rat cortical bone: physiologic differences in different sites of the same tibia. *J Bone Miner Res*, 7:S429–S432.

[19] Compston, J., Skingle, L., & Dempster, D.W. (2018). Bone Histomorphometry. In: Feldman D. (ed) Vitamin D: Fourth Edition, 4th edn. *Academic Press*, New York, pp 959–973.

[20] Ballarre, J., Desimone, P., Chorro, M., & Baca, M. (2013). Bone quality around bioactive silica-based coated stainless steel implants: Analysis by Micro-Raman, XRF and XAS techniques. *J Struct*, 184:164–172.

[21] Hoerth, R.M., Katunar, M.R., Gomez Sanchez, A., et al. (2014). A comparative study of zirconium and titanium implants in rat: osseointegration and bone material quality. *J Mater Sci Mater Med*, 25:411–422.

[22] Awonusi, A., Morris M.D., & Tecklenburg, M.M.J. (2007). Carbonate assignment and calibration in the Raman spectrum of apatite. *Calcif Tissue Int*, 81:46–52.

[23] Yerramshetty, J.S., & Akkus, O. (2008). The associations between mineral crystallinity and the mechanical properties of human cortical bone. *Bone*, 42:476–482.

[24] Kurien, B.T., & Scofield, R.H. (1999). Mouse urine collection using clear plastic wrap. *Lab Anim*, 33:83–86.

[25] Voigt, G.L. (2000). Hematology techniques and concepts for veterinary technicians. *John Wiley & Sons*, IA, USA.

[26] Hulsart-Billström, G., Dawson, J.I., Hofmann, S., et al. (2016). A surprisingly poor correlation between in vitro and in vivo testing of biomaterials for bone regeneration: Results of a multicentre analysis. *Eur Cells Mater*, 31:312–322.

[27] Shuai, C., Li S., Peng, S., et al. (2019). Biodegradable metallic bone implants. *Mater Chem Front*, 3:544–562.

[28] Khan, A.R., Grewal, N.S., Zhou, C., et al. (2023). Recent advances in biodegradable metals for implant applications: Exploring in vivo and in vitro responses. *Results Eng*, 20:101526.

[29] Shapiro, F. (2008). Bone development and its relation to fracture repair. The role of mesenchymal osteoblasts and surface osteoblasts. *Eur Cell Mater*, 15:e76.

[30] Steele, J.G., McFarland, C., Dalton, B.A., et al. (1994). Attachment of human bone cells to tissue culture polystyrene and to unmodified polystyrene: the effect of surface chemistry upon initial cell attachment. *J Biomater Sci*, 5:245–257.

[31] Javed, F., Romanos, G.E. (2010). The role of primary stability for successful immediate loading of dental implants. A literature review. *J Dent*, 38:612–620.

[32] Shalabi, M.M., Gortemaker, A., Hof M.V.T., et al. (2006). Implant surface roughness and bone healing: a systematic review. *J Dent Res*, 85:496–500.

[33] Rougerie, P., Silva dos Santos, R., Farina, M., & Anselme, K. (2021). Molecular mechanisms of topography sensing by osteoblasts: an update. *Appl Sci*, 11:1791.

[34] Çehreli, M., Şahin, S., & Akça, K. (2004). Role of mechanical environment and implant design on bone tissue differentiation: current knowledge and future contexts. *J Dent*, 32:123–132.

[35] Wang, J., Ma, X.Y., Feng, Y.F., et al. (2017). Magnesium ions promote the biological behaviour of rat calvarial osteoblasts by activating the PI3K/Akt signalling pathway. *Biol Trace Elem Res*, 179:284–293.

[36] Liu, W., Guo, S., Tang, Z., et al. (2020). Magnesium promotes bone formation and angiogenesis by enhancing MC3T3-E1 secretion of PDGF-BB. *Biochem Biophys Res Commun*, 528:664–670.

[37] Witte, F., Kaese, V., Haferkamp, H., et al. (2005). In vivo corrosion of four magnesium alloys and the associated bone response. *Biomaterials*, 26:3557–3563.

[38] Kawamura, N., Nakao, Y., Ishikawa, R., et al. (2020). Degradation and biocompatibility of AZ31 magnesium alloy implants in vitro and in vivo: a micro-computed tomography study in rats. *Materials (Basel)*, 13:473.

[39] Castellani, C., Lindtner, R.A., Hausbrandt, P., et al. (2011). Bone–implant interface strength and osseointegration: Biodegradable magnesium alloy versus standard titanium control. *Acta Biomater*, 7:432–440.

[40] Katunar, M.R., Gomez Sanchez, A., Santos Coquillat A., et al. (2017). In vitro and in vivo characterization of anodised zirconium as a potential material for biomedical applications. *Mater Sci Eng C*, 75:957–968.

[41] Xin, H., Shi, Q., Ning, X., et al. (2023). Biomimetic mineralized fiber bundle-inspired scaffolding surface on polyetheretherketone implants promotes osseointegration. *Macromol Biosci*, 23:2200436.

[42] Morris, M.D., & Mandair, G.S. (2011). Raman assessment of bone quality. In: Clinical Orthopaedics and Related Research. *Springer New York LLC*, pp 2160–2169.

[43] Kazanci, M., Roschger, P., Paschalis, E.P., et al. (2006). Bone osteonal tissues by Raman spectral mapping: Orientation-composition. *J Struct Biol*, 156:489–496.

[44] Ross, M.H., & Pawlina, W. (2006). Histology: A text and atlas: with correlated cell and molecular biology, 7th edn. *Wolters Kluwer*, China.

[45] Timlin, J.A., Carden, A., & Morris, M.D. (1999). Chemical microstructure of cortical bone probed by Raman transects. *Appl Spectrosc*, 53:1429–1435.

[46] Dziuba, D., Meyer-Lindenberg, A., Seitz, J., & Waizy, H. (2013). Long-term in vivo degradation behaviour and biocompatibility of the magnesium alloy ZEK100 for use as a biodegradable bone implant. *Acta Biomater*, 9:8548–8560.

[47] Zhang, E., Xu, L., Yu, G., et al. (2009). In vivo evaluation of biodegradable magnesium alloy bone implant in the first 6 months implantation. *J Biomed Mater Res A*, 90:882–893.

[48] Hermawan, H., Dubé, D., & Mantovani, D. (2010). Developments in metallic biodegradable stents. *Acta Biomater*, 6:1693–1697.

[49] Zheng, Y., Gu, X., & Witte, F. (2014). Biodegradable metals. *Mater Sci Eng Reports*, 77:1–34.